Pergamon

0301-9322(94)00042-5

Int. J. Multiphase Flow Vol. 20, No. 6, pp. 1095–1107, 1994

0301-9322/94 $7.00 + 0.00

LIQUID SINGLE- AND GAS–LIQUID TWO-PHASE FLOWS OF MAGNETIC FLUID IN THE PRESENCE OF A HIGH NON-UNIFORM PARALLEL MAGNETIC FIELD

M. TAKAHASHI, Y. YAMAZAKI and A. INOUE

Research Laboratory for Nuclear Reactors, Tokyo Institute of Technology, 2-12-1 O-okayama, Meguro-ku, Tokyo 152, Japan

(Received 20 August 1993; in revised form 29 April 1994)

Abstract—The effect of a non-uniform parallel high magnetic field on flow control characteristics is investigated experimentally for a magnetic fluid single-phase flow and an air–magnetic fluid two-phase flow in a vertical channel. It is found that as the magnetic field strength is increased, the friction factor of the single-phase flow increases significantly. For the two-phase flow, the friction pressure loss and the head pressure loss, which is smaller than the friction loss, are negligibly small compared with the magnetic pressure loss. In the case where air is injected $27.9d$ upstream from the maximum magnetic field, the air flow is blocked by the magnetic force in the entrance of the magnetic field, which leads to increases in both local void fraction and pressure drop there. In the case where air is injected $1.43d$ downstream from the maximum magnetic field, the air flow is accelerated, resulting in a decrease in void fraction and an increase in pressure rise. In the latter case and under the present range of experimental conditions, the magnetic pumping head reaches 0.02 MPa at the highest, and the maximum circulation flow rate reaches twice as high as non-magnetically driven flow rate.

Key Words: magnetic fluid, colloidal solution, magnetic field, flow control, two-phase flow, friction factor, pressure drop, void fraction

1. INTRODUCTION

A magnetic fluid is a stable colloidal solution of superfine magnetic particles suspended in a liquid solvent with a surface active agent. The magnetic fluid is magnetized to be $\mathbf{M}(\mathbf{H})$ in the presence of a magnetic field $\mathbf{H}$. If a non-uniform magnetic field with a gradient $\nabla\mathbf{H}$ is applied to the magnetic fluid, a magnetic body force $\mathbf{F} \equiv \mu_0(\mathbf{M} \cdot \nabla)\mathbf{H}$ acts on the magnetic fluid (Rosensweig 1985, pp. 8–16), where μ_0 is the magnetic permeability in a vacuum. Since the magnetic body force attracts the magnetic fluid towards a higher magnetic field, the fluid is compressed locally in the region of high magnetic field. If the magnetic fluid contains a gas phase, the gas phase is exhausted towards a lower magnetic field by the magnetic body force.

The use of this magnetic force makes it possible to realize various types of two-phase flow control which have been impossible without magnetic fluid. For example, the magnetic fluid seal (Rosensweig 1985, pp. 142–146) is considered as one of such two-phase flow controls, since a magnetic fluid is strongly attracted by magnet poles and the seal is maintained under ordinary conditions, but if a pressure difference exceeds a burst pressure, gas flows through the seal in a two-phase flow as shown in figure 1(a) (Sato 1988).

Another example is a gas lift pump driven by the magnetically exhausted gas flow which has been proposed by Kamiyama & Ishikawa (1989) and Kamiyama (1992). As shown in figure 1(b), when gas is injected or formed by boiling in the region where a magnetic field with a negative field gradient is applied, the gas-phase is exhausted in the flow direction by the magnetic force, and this gas flow induces the circulation of the working fluid. It should be noted that a two-phase flow starts in the region where a magnetic field is applied. It has been expected that this pump is applied to the liquid metal MHD power generation system by using a liquid metal-based magnetic fluid as a working fluid.

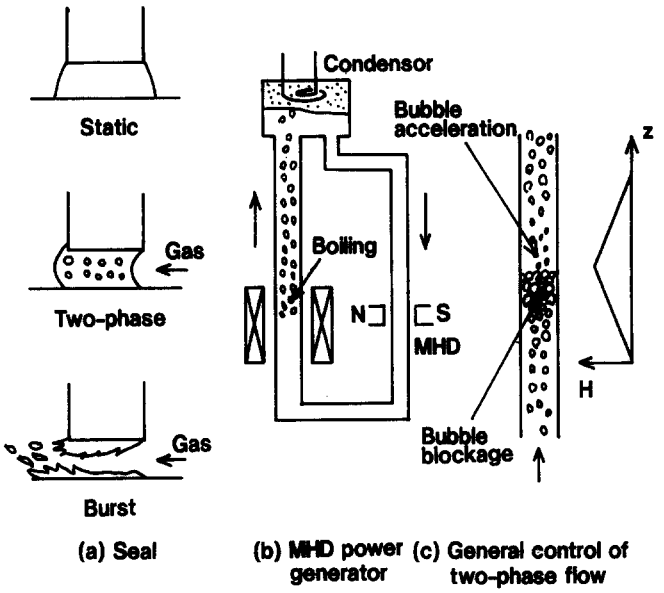

Figure 1. Two-phase flow control.

As a fundamental study of this system, the flow characteristics of a gas–magnetic fluid two-phase flow were investigated for the cases of gas injection (Kamiyama & Inoue 1988; Kamiyama & Ishikawa 1989; Kamiyama 1992) and boiling (Kamiyama & Okubo 1991; Kamiyama *et al.* 1992). In these studies, the two-phase flow starting from the throat of a contracted nozzle was dealt with. Related to this system, the effect of a field gradient on the boiling behaviors of magnetic fluids in the boiling position was also studied by Takahashi *et al.* (1993).

The magnetic fluid seal and the gas lift pump mentioned above may be specific cases of the two-phase flow control realized by using magnetic fluids. As a more general case, it is interesting to investigate the magnetic fluid two-phase flow in a straight circular channel in an axially non-uniform magnetic field shown in figure 1(c). In the region where the magnetic field has a positive gradient in the flow direction, the magnetic force acts on the fluid in the flow direction. As a result of this body force, a gas flow is decelerated, and the blockage of gas flow having a large magnetic pressure drop may appear there. In the region where the field has a negative gradient in the flow direction, the magnetic force acts on the magnetic fluid upstream, which accelerates the gas flow in the flow direction. The accelerated gas flow increases the gas–liquid slip ratio and the pressure rises in the flow direction, which means a pumping effect.

The problems are how the void fraction and the pressure drop increase in the gas blockage region, and how the void fraction decreases and the pressure rise increases in the gas acceleration region. In addition, it is interesting what flow rate and pump head the magnetically driven gas lift pump has if a more than one-order higher magnetic field than those of the previous studies (Kamiyama & Inoue 1988; Kamiyama & Ishikawa 1989; Kamiyama & Okubo 1991; Kamiyama *et al.* 1992) is applied to the gas injection region.

Thus, the present study deals with this fundamental gas–magnetic fluid two-phase flow system in a vertical straight circular channel in the presence of an axially non-uniform magnetic field. A superconducting magnet is used to apply the magnetic field up to the strength of 4.78 MA/m (the magnetic flux density of 6 T). The study consists of three experiments: (1) gas is injected far upstream from the applied magnetic field region in order to investigate the combined behaviors of both gas blockage and gas acceleration occurring upstream and downstream from the maximum magnetic field, respectively; (2) gas is injected in the region where the applied magnetic field has an axially negative gradient of the field strength in order to investigate the behaviors of the gas acceleration alone; and (3) the performance of the magnetically driven gas lift pump is investigated by using a natural circulation loop without an external pump.

Table 1. Magnetic fluid

Material of particles	Magnetite(Fe_3O_4)
Solvent	Kerosene
Surfactant	Olein acid
Concentration	30.0 wt%
Density	1070 kg/m^3
Viscosity	3600 μPas
Surface tension	25.7 mN/m
Magnetization at 3.2×10^4 A/m	1.64×10^4 A/m

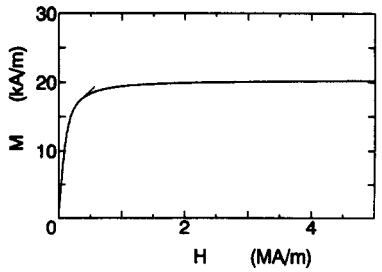

Figure 2. Magnetization of magnetic fluid.

2. EXPERIMENTAL APPARATUS, PROCEDURE, AND DEFINITION OF MEASURED PROPERTIES

2.1. Experimental apparatus and procedure

The magnetic fluid used was a colloidal solution of magnetite particles (Fe_3O_4) about 10 nm in size which were stably dispersed in kerosene with a surface active agent of olein acid. This magnetic fluid was chosen for the present experiment because the vapor pressure was low at the room temperature, and did not have the problem of bubbling and blow-up due to the separation of surface active agent which appeared in water-based magnetic fluid. The specifications and physical properties of the magnetic fluid are presented in table 1. Figure 2 shows the magnetization of the magnetic fluid M in a magnetic field of strength H. This curve consisted of the data measured in a magnetic field $H < 0.80$ MA/m, and it was extrapolated to a higher magnetic field up to $H = 5$ MA/m using the Langevin function (Rosensweig 1985, p.58). Air was used as a gas phase.

Figure 3 shows a schematic diagram of the air–magnetic fluid two-phase flow loop and a solenoidal superconducting magnet. The magnetic fluid flow, which was driven by the diaphragm pump, passed through the pulsation damper, the orifice flow meter and then the test channel. The

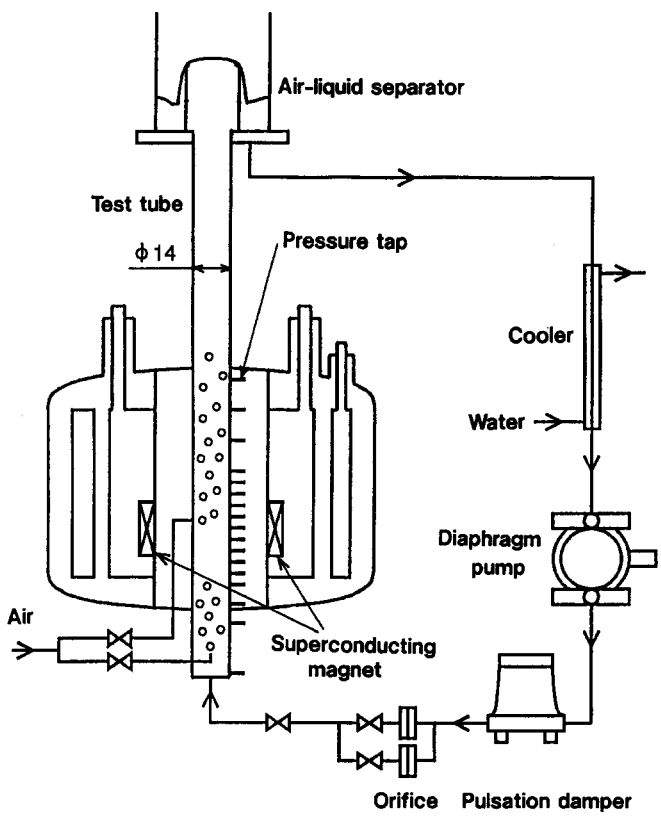

Figure 3. Schematic diagram of air–magnetic fluid two-phase flow loop.

air supplied by a compressor passed through a pressure regulating valve and a flow meter made of SS-304 fine tubes, and then entered the test channel through air injectors. The two-phase mixture from the test channel entered the gas–liquid separator, and the air was discharged to the atmosphere. The magnetic fluid returned to the pump after passing through the water cooler in which the fluid temperature was controlled.

The superconducting magnet used was a vertical NbTi solenoidal magnet. The axial length of magnet coil was 200 mm, the maximum magnetic field strength was 5.57 MA/m (70 kOe) and the inner diameter of the air bore was 76 mm. The orientation of the magnetic field lines was approximately parallel to the axis of the test channel. An axially non-uniform magnetic field was applied to the test channel by this magnet.

Figure 4 shows a schematic of the test section which was a vertical circular channel made of SS-304 14 mm in inner diameter d. The test channel was co-axially set in the center of the magnet air bore. The pressure taps indicated by P_{in}, $P_1 \sim P_{16}$ were made of holes 1 mm in diameter on the inside surface of the channel. The pressures at the taps were introduced to the electric differential pressure transducers through SS-304 tubes 4 mm in outer diameter. The tubes were filled with the magnetic fluid.

The axial distributions of the applied magnetic field strength computed in the bore center are shown in figure 5. The maximum magnetic field strength of 4.78 MA/m (60 kOe) corresponds to the magnetic flux density of 6 teslas.

In the first experiment, the air injector was inserted horizontally at the location A1 which was 27.9 d (0.39 m) upstream from the maximum magnetic field. The air injector was made of a pipe SS-304 4 mm in diameter, the upper half of which was cut and covered with meshes to inject small bubbles in a uniform size.

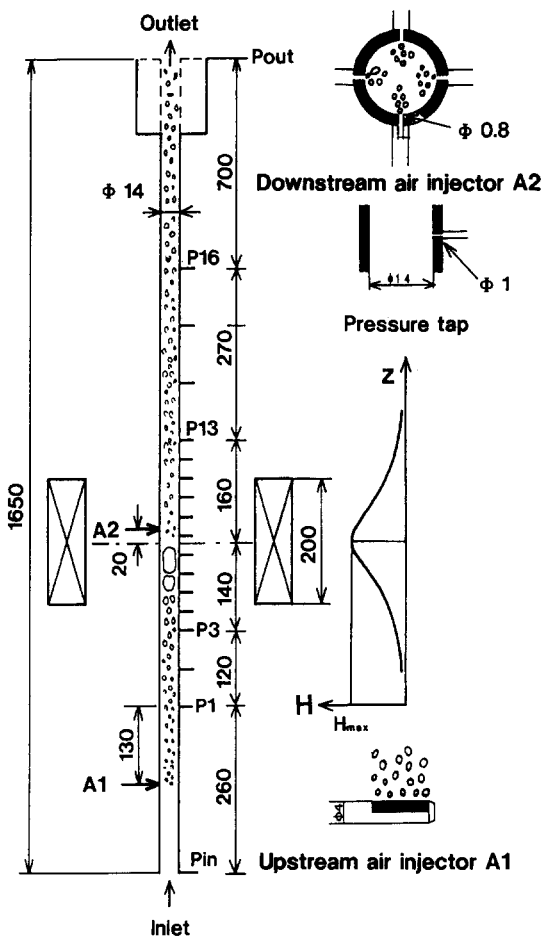

Figure 4. Schematic of test section.

In the second and third experiments, air was injected at A2 which was located 1.43 d (20 mm) downstream from the maximum magnetic field, and 1.79 d (25 mm) upstream from the maximum magnetic field gradient. This was chosen so as to accelerate the air as effectively as possible by letting it pass through a magnetic field with maximum negative gradient. The injector was made of four holes 0.8 mm in diameter on the inner surface of the channel arranged peripherally at equal intervals.

2.2. *Measured properties*

The pressure drop ΔP consists of the friction pressure loss ΔP_f, the head loss ΔP_h, the acceleration loss ΔP_a and the magnetic pressure drop ΔP_m as,

$$\Delta P = \Delta P_f + \Delta P_h + \Delta P_a + \Delta P_m. \quad [1]$$

Here, the magnetic pressure drop and the head loss are given by,

$$\Delta P_m \equiv -\mu_0 \int_{H_i}^{H_j} (1-\epsilon) M \, dH, \quad [2]$$

$$\Delta P_h \equiv [\rho_G \epsilon + \rho_L (1-\epsilon)] g L_{i-j}, \quad [3]$$

where ρ_G and ρ_L are the densities of air and magnetic fluid, respectively, ϵ is the local void fraction, L_{i-j} is the axial distance between P_i and P_j, g is the gravitational acceleration and H_i and H_j are the magnetic field strength at P_i and P_j, respectively. The measured properties are described below based on [1]–[3].

(a) Friction factor in the single-phase flow of magnetic fluid. For a magnetic fluid single-phase flow, the friction loss ΔP_f was directly measured by the differential pressure transducer, since ΔP_a was negligibly small in the straight channel, and both $\Delta P_h \equiv \rho_L g z$ and $\Delta P_m \equiv -\mu_0 \int_{H_i}^{H_j} M dH$ in the test channel were balanced with those in the tubes from the pressure taps to the pressure transducers. It is also noted that the magnetic pressure drop upstream from the maximum magnetic field was negative, and the magnetic pressure drop downstream from it was positive, and hence the sum of them from the inlet to the outlet far outside of the magnetic field region ΔP_m was equal to zero.

From the measured pressure drop, the friction factor λ defined by,

$$\Delta P_f = \lambda \frac{1}{2} \rho_L V_L^2 \frac{L_{1-out}}{d}, \quad [4]$$

was determined, where V_L was the average velocity of the magnetic fluid in the test channel, and L_{1-out} was the axial distance between P_1 and P_{out}.

(b) Average void fraction in the two-phase flow. The channel average void fractions from the air injection point to the free surface $\langle \epsilon \rangle$ were measured by means of the quick shut method. A cylindrical block was inserted into the inner tube of the gas–liquid separator to make the channel cross section uniform in the whole of the channel.

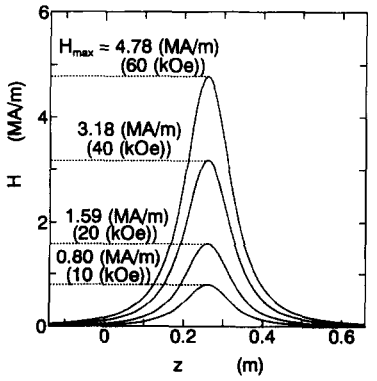

Figure 5. Axial distributions of applied magnetic field calculated.

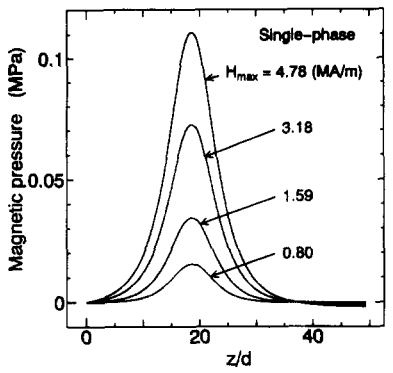

Figure 6. Axial distributions of magnetic pressure calculated in a single-phase magnetic fluid.

(c) Axial pressure distribution in the two-phase flow. The pressure distribution P_i with the reference pressure P_1 expressed by,

$$P_i - P_1 = -[\Delta P_f + \Delta P_h + \Delta P_a + \Delta P_m]_1^i, \qquad [5a]$$

was measured. Since the local void fraction ϵ was not measured in the present experiment, ΔP_f, ΔP_h, ΔP_a and ΔP_m could not be estimated independently. The substitution of [2] and [3] into [5a] gives,

$$P_i - P_1 = -\Delta P_f - \Delta P_a + [(\rho_L - \rho_G)\epsilon - \rho_L]gz + \mu_0 \int_{H_1}^{H_i} (1-\epsilon) M \mathrm{d}H. \qquad [5b]$$

For the case that the test channel is filled with the magnetic fluid, that is $\epsilon = 0$, the magnetic pressure in the test section was calculated from the magnetization M in figure 2 and the applied magnetic field H in figure 5. The result is shown in figure 6. Here, the magnetic pressure is negative at $z/d \geqslant 37$, since H_1 at the reference point is not zero. The magnetic pressure loss was much larger than the other three losses under the present experimental conditions.

If the half of the channel from the inlet to the point of the maximum magnetic field was filled with magnetic fluid and the other half was filled with air, the magnetic pressure drop should be the maximum: $\mu_0 \int_0^{H_{max}} M \mathrm{d}H$. On the other hand, if the half of the channel from the inlet to the point of the maximum magnetic field were filled with air and the other half were filled with magnetic fluid, the magnetic pressure rise should become the same maximum value. Thus, the pressure coefficient C_m was defined by,

$$C_m = \frac{P_i - \mathrm{P}_1 + \rho_L g z}{\mu_0 \int_0^{H_{max}} M \mathrm{d}H}. \qquad [6]$$

for the measure of the measured pressure loss or rise to the possible maximum magnetic pressure drop or rise. C_m was defined with $P_i - \mathrm{P}_1 + \rho_L g z$, since it provided better non-dimensional unified curves than that with $P_i - P_1$ particularly in the region $z/d < 30$ as shown later in figure 16(b).

(d) Total pressure drop and total pressure rise in the two-phase flow. The total pressure drop from P_{in} to P_{out} is expressed as,

$$\Delta P_t = [\Delta P_f + \Delta P_a + \Delta P_h + \Delta P_m]_{in}^{out}. \qquad [7]$$

The total pressure rise coefficient $[C_m]_t$ was defined by,

$$[C_m]_t = -\frac{\Delta P_t}{\mu_0 \int_0^{H_{max}} M \mathrm{d}H}. \qquad [8]$$

while the total pressure drop coefficient was given by $-[C_m]_t$.

(e) Resistance coefficient of the circulation loop. For the evaluation of the performance of the magnetically driven gas lift pump, the magnetic fluid circulation loop which did not have the pump

Table 2. Experimental conditions

System pressure, P		0.1 MPa
Superficial velocity	Magnetic fluid, V_{L0}	0.13–1.0 m/s
	Air, V_{G0}	0–3.0 m/s
Magnetic field strength, H		0–4.78 MA/m (0–60 kOe)

and the damper was used, and air was injected into the region having a negative magnetic field gradient. Prior to this experiment, the flow resistance coefficient of the loop ξ defined by,

$$\xi = \frac{P_1 - P_{out}}{\frac{1}{2}\rho_L V_{L0}^2}, \quad [9]$$

was determined, where V_{L0} was the superficial velocity of the magnetic fluid in the test channel.

2.3. *Experimental conditions and experimental error*

The experimental conditions are shown in table 2. The system pressure in the gas–liquid separator P_{out} was set 0.1 MPa. The fluid temperature was maintained at 10°C.

From the observation of an air–kerosene two-phase flow, it was expected that the air–magnetic fluid two-phase flow belonged to the bubbly and slug flow regime, although the physical properties of the magnetic fluid were somewhat different from those of kerosene, that is, the density 823 kg/m^3 and the viscosity 1763 μPa s of kerosene at 10°C are lower than those of the magnetic fluid.

The experimental errors of the air and magnetic fluid flow rates and the pressure difference were within $\pm 2\%$. The amount of measured data scatter due to the fluctuation of the two-phase flow was estimated to be approximately $\pm 5\%$ at the maximum for both the pressure difference and void fraction.

3. EXPERIMENTAL RESULTS AND DISCUSSION

3.1. *Friction pressure losses of single- and two-phase flows*

3.1.1. Friction factor of single-phase flow. Figure 7 shows the experimental result for the friction factor λ in a magnetic fluid single-phase flow, where Re ($\equiv \rho_L V_L d/\eta$) is the Reynolds number and H_{max} is the peak value of the axial distribution of the magnetic field strength. It is found that the slope of the data curve is slightly gentler than the slope of the laminar flow correlation $\lambda = 64/\mathrm{Re}$ in the absence of a magnetic field. Above Re = 3000, the data curve approaches the curve of the Blasius correlation $\lambda = 0.3164/\mathrm{Re}^{0.25}$ for a turbulent flow. As the magnetic field is applied and increased, λ increases in the range of Re $\leqslant$ 3000, and the slope becomes steeper and nearly parallel to the laminar flows. The slope also becomes steeper in the range of Re $\geqslant$ 3000. It is interesting that λ decreases when H_{max} is increased beyond 3.18 MA/m. These results suggest that the application of a magnetic field laminarizes the magnetic fluid flow.

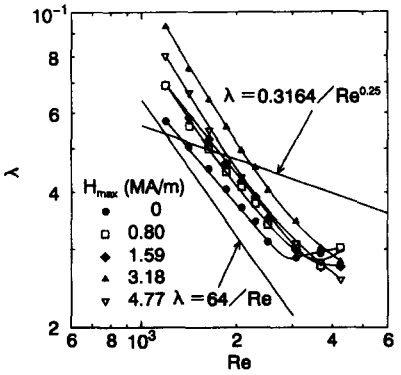

Figure 7. Friction factor in a single-phase flow of magnetic fluid.

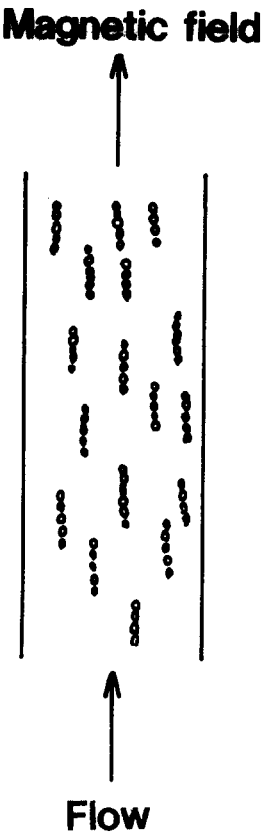

Figure 8. Clusters formed in axial magnetic field.

Similar increases in λ were reported by Kamiyama *et al.* (1979) and by Kamiyama *et al.* (1981) for the laminar pipe flow of a water-based magnetic fluid under parallel and transverse magnetic fields, respectively. However, since the applied magnetic field in the present study was more than one order higher than those in these studies, the increase in λ in the present data is much larger than these previous results.

The possible reason for the increase in the friction loss may be the viscosity increase in a magnetic field due to the suppression of particle rotations (Shliomis 1967; Kamiyama *et al.* 1979, 1981) or due to the formation of clusters (Kamiyama *et al.* 1986; Kamiyama & Satoh 1988). The cluster formation model is schematically illustrated in figure 8. The model of the suppression of particle rotations predicted the experimental result of viscosity increase in a water-based magnetic fluid under a parallel magnetic field and that of a hydrocarbon-based magnetic fluid. However, it was found that the cluster formation model was capable of explaining the large viscosity increase observed in the previous studies better than the particle rotation model. Therefore, the present result is also attributed to the formation of clusters.

3.1.2. Friction pressure loss of two-phase flow. The friction pressure loss of the two-phase flow was not determined independently from our measured pressures, since the measuring technique of local void fraction ϵ in a magnetic fluid had not been established yet. Thus, it was order-estimated by means of the Lockhart–Martinelli method as follows.

In the case of the air injection upstream ($V_{G0} = 0.425$ m/s and $V_{L0} = 0.392$ m/s), the Lockhart–Martinelli parameter $\chi \equiv (\Delta P_{L0}/\Delta P_{G0})^{1/2}$ is estimated to be 15.4, and then the friction multiplier $\phi_L^2 \equiv \Delta P_f/\Delta P_{L0}$ is 2.37 according to the Chisholm correlation. Here, V_{L0} and V_{G0} are the air and magnetic fluid superficial velocities, and ΔP_{L0} and ΔP_{G0} are the friction pressure losses of magnetic fluid and air single-phase flows, respectively. The experimental result that $\lambda \simeq 0.05$–0.07 at Re = 1633 shown in figure 7 gives the pressure difference $\Delta P_f \equiv \phi_L^2 \lambda \rho_L V_{L0}^2 z/2d = (19.6\text{–}13.6)z/d$ Pa which leads to $\Delta P_f \simeq 0.49$–0.68 kPa at $z/d = 50$. This friction pressure difference is 10–14% of the total change in $P_i - P_1$ which will be shown later in figure 10. As a result, it is found that the head

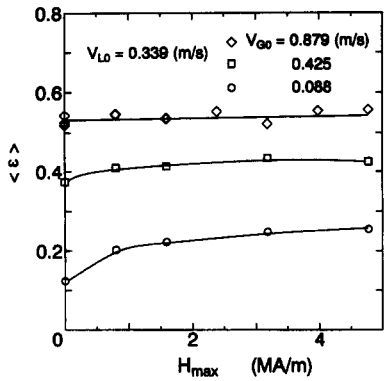

Figure 9. Channel average void fractions between air injection point and free surface for air injection upstream.

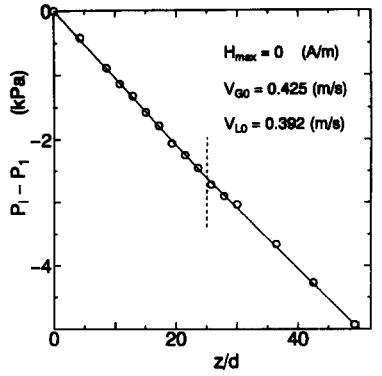

Figure 10. Axial pressure coefficient distribution for air injection at A1 in absence of magnetic field.

loss is approximately 3–4 times as high as the friction loss, taking into account that the acceleration loss is negligibly small.

Similarly, in the case that air is injected downstream ($V_{G0} = 1.24$ m/s and $V_{L0} = 0.550$ m/s), χ is equal to 12.0, which corresponds to $\phi_L^2 = 2.76$. Since $\lambda \simeq 0.035$–0.05 at Re = 2291 in figure 7, $\Delta P_f \simeq (15.7\text{–}22.7) z/d$ Pa, which is 13–19% of the total pressure drop at $z/d = 50$ which will be shown later in figure 15. Hence, the head loss is approximately 2–3 times as high as the friction loss, taking into account that the acceleration loss is negligibly small except for those near the air injection point.

3.2. Flow characteristics of two-phase flow with air injection upstream

The experimental result for the flow characteristics of the air–magnetic fluid two-phase flow with the air injection upstream is described below.

3.2.1. Channel average void fraction. Figure 9 shows the dependence of the measured channel average void fraction $\langle \epsilon \rangle$ on the maximum magnetic field H_{max}. It is found that the void fraction increases with increasing H_{max} up to about 3 MA/m both for $V_{G0} = 0.088$ m/s and 0.425 m/s, but it is not influenced by the magnetic field for $V_{G0} = 0.878$ m/s. As V_{G0} is decreased, the increase in $\langle \epsilon \rangle$ is more significant. From these results, it is found that as a result of the magnetic body force which acts on the magnetic fluid, air flow is decelerated and blocked in the region where $dH/dz \geqslant 0$. At $V_{G0} = 0.425$ where the flow belongs to a bubbly flow according to the flow regime map, it is possible that the air phase resides and coalesces in the decelerated region.

3.2.2. Axial pressure distribution. Figure 10 shows the measured axial pressure distribution $P_i - P_1$ in the absence of a magnetic field. It is found that P_i decreases linearly with z/d, following the forth term of [5b], since the head loss is dominant as mentioned in section 3.1.2. The change in the slope at $z/d \simeq 25$ may be caused by a slight change in flow pattern there.

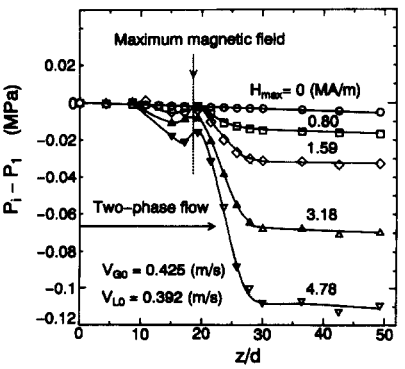

Figure 11(a). Axial pressure distributions for air injection upstream from magnetic field, A1.

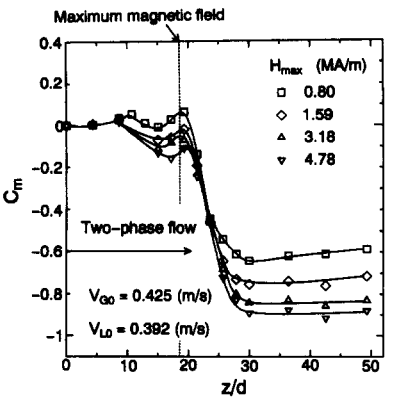

Figure 11(b). Axial pressure distributions normalized by maximum magnetic pressure for air injection upstream from magnetic field, A1.

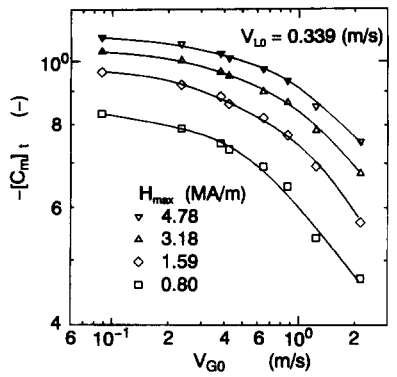

Figure 12. Dimensionless pressure drop normalized by maximum magnetic pressure.

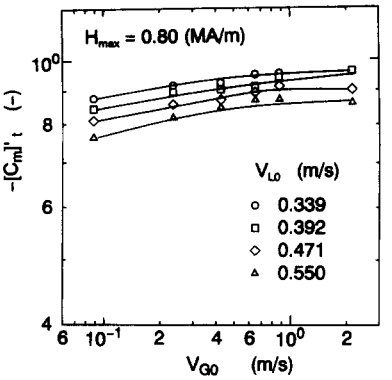

Figure 13. Dimensionless pressure drop normalized by maximum magnetic pressure upstream from maximum magnetic field.

Figure 11(a) shows the axial pressure distributions $P_i - P_1$ in the presence of a magnetic field. The comparison of curves at $H_{max} = 0$ and $H_{max} = 0.80$–4.78 MA/m indicates that the magnetic pressure loss is much higher than the friction and head losses.

This magnetic pressure is dominated by the local void fraction according to the last term of [5b], that is, the pressure distributions may represent the axial distributions of the local void fraction. As shown in figure 11(a), $P_i - P_1$ changes a little upstream from the maximum magnetic field, and drops greatly downstream from it. These curves of $P_i - P_1$ indicate that the local void fraction is larger upstream from the maximum magnetic field. From these results, it is apparent that the blockage of air flow is formed there. Similarly, the curves of $P_i - P_1$ downstream from the maximum magnetic field indicate that the local void fraction is smaller there. This means that the air flow is accelerated there. The values of $P_i - P_1$ becomes nearly constant in the flow direction in the regions $z/d \leqslant 10$ and $z/d \geqslant 30$, since the magnitude of a magnetic field gradient $|dH/dz|$ is much lower there.

From the values of $P_i - P_1$ downstream, it is found that the total flow resistance obtained by the magnetic force reaches 0.017–0.11 MPa for $H_{max} = 0.80$–4.77 MA/m. Figure 11(b) shows the axial distributions of the pressure coefficient C_m. It is found that this flow resistance corresponds to 60–90% of the possible maximum magnetic pressure drop in this flow system. The value of C_m becomes higher for higher H_{max} in the region where $z/d > 30$, that is, the reduction of flow resistance effect. This is possibly because the air phase is compressed and accelerated more and as a result the local void fraction is decreased by the increased magnetic effect downstream from the maximum magnetic field.

3.2.3. Total pressure drop. Figure 12 shows the measured dimensionless total pressure drop $-[C_m]_t$ defined by [8]. It is found that $-[C_m]_t$ increases with increasing H_{max} and decreasing V_{G0}. The total pressure drop is considered as the sum of the magnetic pressure drop due to air blockage

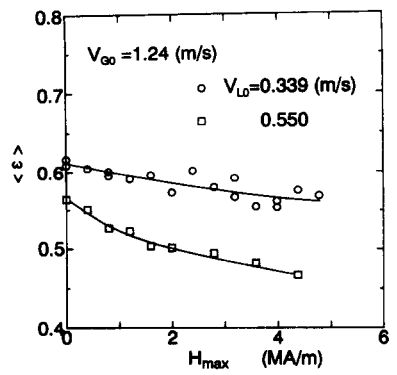

Figure 14. Channel average void fractions between air injection point and free surface for air injection downstream from maximum magnetic field.

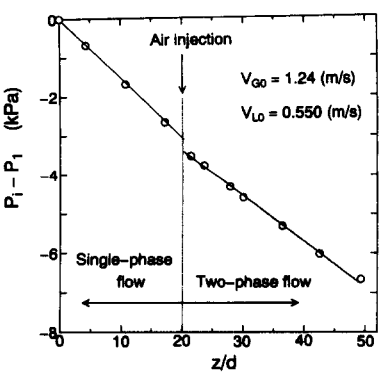

Figure 15. Axial pressure distribution for air injection A2 in absence of magnetic field.

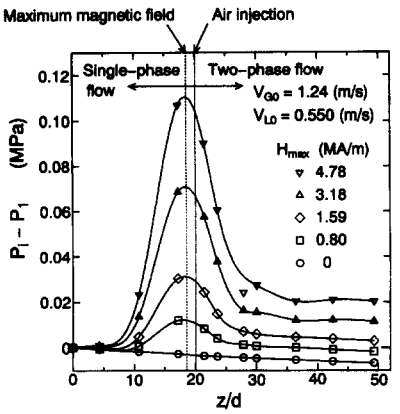

Figure 16(a). Axial pressure distributions for air injection downstream from maximum magnetic field, A2.

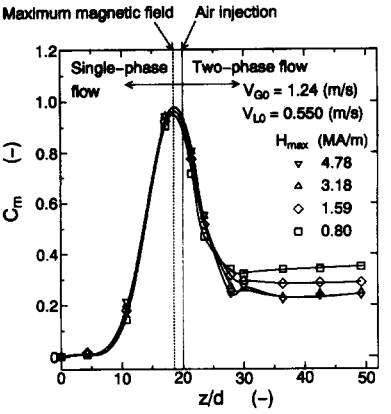

Figure 16(b). Pressure coefficient distributions normalized by maximum magnetic pressure for air injection, A2.

upstream and the magnetic pressure rise downstream. The magnetic pressure drop upstream can be separately estimated, if the magnetic pressure rise downstream given in figure 17 of section 3.3.3. is subtracted from the total pressure drop given in figure 12. The result denoted by $-[C_m]_t'$ is shown in figure 13. It is found that the dependence of $-[C_m]_t'$ on V_{G0} and V_{L0} is greatly reduced compared with $-[C_m]_t$ shown in figure 12, and the pressure drop upstream reaches 75–100% of the possible maximum magnetic pressure drop.

3.3. Flow characteristics of two-phase flow with air injection downstream

The experimental result for the flow characteristics of the air–magnetic fluid two-phase flow with air injection downstream is described below.

3.3.1. Channel average void fraction. Figure 14 shows the dependence of the measured channel average void fraction $\langle \epsilon \rangle$ on magnetic field strength. The fact that as H_{max} increases, $\langle \epsilon \rangle$ decreases appreciably, suggests that the air flow is accelerated and then the local void fraction decreases in the region where $dH/dz \leqslant 0$ as a result of the magnetic body force acting on the magnetic fluid. The decreasing rate becomes lower with increasing H_{max} and with decreasing V_{L0}.

3.3.2. Axial pressure distribution. Figure 15 shows the measured axial pressure distribution $P_i - P_1$ in the absence of magnetic field. It is found that $P_i - P_1$ decreases linearly with z/d in a single-phase flow upstream from the air injection position due to the friction and head pressure losses. The discontinuous drop of $P_i - P_1$ appearing near the air injection position may be caused by the acceleration loss. In the region $z/d > 22$ where the flow is a two-phase one, $P_i - P_1$ decreases linearly with z/d, following the two-phase friction and head losses expressed by [5b].

Figure 16(a) shows the pressure distributions $P_i - P_1$. It is found that $P_i - P_1$ in the absence of a magnetic field is much smaller than those in the presence of a magnetic field, which means that the magnetic pressure loss is much higher than the friction, acceleration and head losses. It can

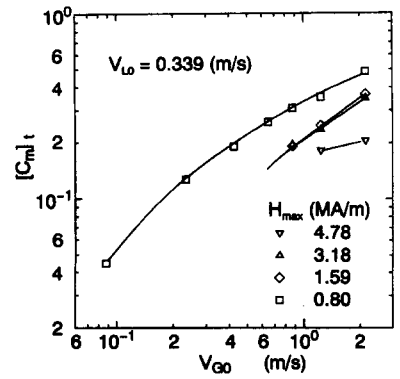

Figure 17. Dimensionless pressure rise normalized by maximum magnetic pressure for air injection, A2.

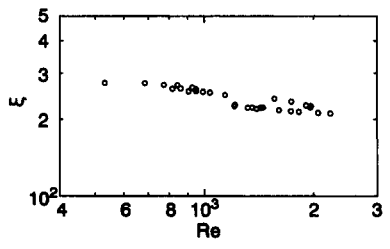

Figure 18. Resistance coefficient of flow loop.

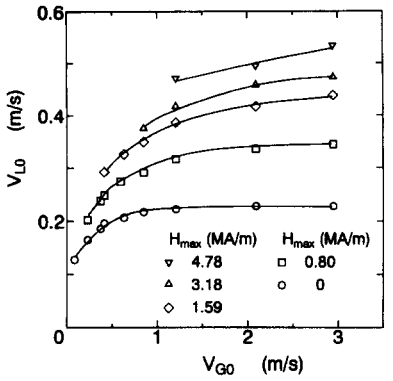

Figure 19. Magnetically driven circulation velocity.

be seen that with increasing z/d, $P_i - P_1$ increases, reaches the maximum at the position of the maximum magnetic field, then decreases and finally becomes constant in the region $z/d > 35$. It is found that the decrease in $P_i - P_1$ downstream is reduced more as H_{max} increases. The total pressure rise corresponding to pump head reaches 0.02 MPa at $H_{max} = 4.78$ MA/m.

The measured axial distributions of C_m are shown in figure 16(b). It is found that all the curves for the different values of H_{max} are nearly the same up to $z/d = 25$. However, in the region where $z/d > 25$, as H_{max} is higher, $P_i - P_1$ becomes lower, possibly because the air flow is more accelerated and compressed, and then the void fraction which influences the pressure rise decreases. In other words, the efficiency of magnetic pumping effect is reduced by increasing the magnetic field strength.

3.3.3. Total pressure rise. Figure 17 shows the measured dimensionless total pressure rise $[C_m]_t$. It is found that $[C_m]_t$ increases with decreasing H_{max} and increasing V_{G0}, the latter of which is attributed to the increase in void fraction. It is found that the maximum value of $[C_m]_t$ is approximately 0.5, indicating that the pressure rise or the pump head reaching 50% of the possible maximum magnetic pressure rise is obtained in the present flow system.

3.3.4. Magnetic pumping performance. In order to investigate the magnetic pumping performance, air was injected at A2 as shown in figure 4 and the flow rate of the magnetic fluid was measured using the natural circulation loop without the pump and the pulsation damper. As the flow characteristics of the loop used, the measured flow resistance coefficient ξ defined by [9] which includes all types of single-phase pressure losses except for the head loss is shown in figure 18, where Re is the Reynolds number defined by $\mathrm{Re} \equiv \rho_L d V_{L0}/\eta_L$.

Figure 19 shows the effect of the injected air superficial velocity V_{G0} on the superficial velocity of the magnetic fluid V_{L0} or the circulation flow rate. It is found that the circulation flow rate of the magnetic fluid increases with increasing V_{G0} and reaches 0.21 m/s at the maximum even in the absence of a magnetic field. However, as H_{max} is increased, the circulation flow rate becomes higher and reaches 0.53 m/s at the maximum for the maximum magnetic field and injected air flow rate under the range of the present experiment. This maximum circulation velocity is approximately 2.5 times higher than that in the absence of the magnetic field. This result means that much better pumping performance than the previous studies is achieved by applying more than one order higher magnetic field of 4.78 MA/m.

4. CONCLUSIONS

The flow control characteristics by a non-uniform parallel magnetic field up to 4.78 MA/m were experimentally investigated for the single-phase flow of magnetic fluid and the two-phase flow of air and magnetic fluid in a vertical circular channel. The conclusions are described below.

(1) The friction factor of the single-phase flow increases appreciably as the magnetic field increases.
(2) In the two-phase flow, the magnetic pressure loss is much higher than the friction, head and acceleration pressure losses under the present experimental conditions.
(3) In the case where air is injected upstream from the magnetic field, the channel average void fraction increases with increasing magnetic field, and the pressure drop reaches 0.11 MPa

at the maximum. This is caused by the combination of a blocked air flow upstream from the maximum magnetic field and an accelerated air flow downstream. The maximum pressure drop upstream reaches 75–100% of the possible maximum magnetic pressure drop.

(4) In the case where air is injected downstream from the maximum magnetic field, the void fraction decreases with increasing magnetic field, and the pressure rise of 0.02 MPa is obtained. The pressure rise reaches approximately 50% of the possible maximum magnetic pressure rise at the maximum under the present experimental conditions.

(5) In the case where air is injected downstream from the maximum magnetic field in a circulation loop without a pump, the magnetically driven maximum circulation flow rate is 2.5 times as high as the maximum one driven only by the buoyancy force of air in the absence of a magnetic field.

Acknowledgements—The authors wish to express their gratitude to Mr Katsuaki Kayama and Mr Keizo Matsumura for their technical advice and assistance in the preparation and operation of the superconducting magnet. They are also indebted to Dr Masao Nomura and Mr Mitsuo Matsuzaki for their support and assistance.

REFERENCES

KAMIYAMA, K. & OKUBO, M. 1991 Gas–liquid two-phase flow of magnetic fluids. *Proc. Int. Conf. Multiphase Flows*, Tsukuba, Japan pp. 77–83.

KAMIYAMA, S. 1992 Pipe flow problems of magnetic fluids (Review). *JSME Int. J.* **35,** 131–137.

KAMIYAMA, S. & INOUE, S. 1988 A study on the two-phase flow characteristics of a magnetic fluid. *Trans. JSME* **54B,** 80–86 (in Japanese).

KAMIYAMA, S. & ISHIKAWA, H. 1989 Two-phase flow characteristics of temperature-sensitive magnetic fluid. *Trans, JSME* **55B,** 741–747 (in Japanese).

KAMIYAMA, S.& MOKUYA, K. 1982 Flow of a ferroliquid in an inhomogeneous transverse magnetic field. *Magnetohydrodynamics* **18,** 13–16.

KAMIYAMA, S. & SATOH, A. 1989 Rheological properties of magnetic fluids with the formation of clusters: analysis of simple shear flow in a strong magnetic field. *J. Colloid Interface Sci.* **127,** 173–188.

KAMIYAMA, S., KAMIYA, T. & IZU, H. 1992 Effect of magnetic field on gas–liquid two-phase pipe flow of magnetic fluid. *Proc. Int. Symp. Electromag. Forces Applications*, Sendai, Japan, pp. 87–90. Elsevier, Amsterdam.

KAMIYAMA, S., KOIKE, K. &IIZUKA, N. 1979 On the flow of a ferromagnetic fluid in a circular tube (Report 1, Flow in a uniform magnetic field). *Bull. JSME* **22,** 1205–1211.

KAMIYAMA, S., KOIKE, K. & IIZUKA, N. 1980 On the flow of a ferromagnetic fluid in a circular pipe. *Rep. Inst. High Speed Mech.* **41,** 21–35.

KAMIYAMA, S., KOIKE, K. & WANG, Z. 1987 Rheological characteristics of magnetic fluids. *JSME Int. J.* **30,** 761–766.

KAMIYAMA, S., OYAMA, T. & MOKUYA, K. 1981 On the flow of a ferromagnetic fluid in a circular tube (4th Report, Experimental study of the flow in a nonuniform transverse magnetic field). *Trans. JSME* **47B,** 2299–2305 (in Japanese).

ROSENSWEIG, R. E. 1985 *Ferrohydrodynamics.* Cambridge University Press, Cambridge.

SHLIOMIS, M. I. 1967 Hydrodynamics of a liquid with intrinsic rotation. *Soviet Phys. JETP* **24,** 173–177.

SATO, K. 1988 Characteristics of magnetic fluid seal. *Mach. Design* **32,** 48–53 (in Japanese).

TAKAHASHI, M., SHINBO, K., OHKAWA, R., MATSUZAKI, M. & INOUE, A. 1993 Nucleate pool boiling heat transfer of magnetic fluid in a magnetic field. *J. Mag. Mag. Mater.* **122,** 301–304.

TAKAHASHI, M., INOUE, A., MATSUZAKI, M. & OHKAWA, R. (1994) Saturated pool boiling heat transfer of toluene-solvent magnetic fluid on a horizontal surface (Effects of field gradient, concentration of particles, and pressure). *Heat Transfer, Japanese Res.* (In press).